HHS Public Access

Author manuscript

Mol Pharm. Author manuscript; available in PMC 2021 July 30.

Published in final edited form as:

Mol Pharm. 2020 February 03; 17(2): 392–403. doi:10.1021/acs.molpharmaceut.9b00589.

Extracellular-Matrix-Anchored Click Motifs for Specific Tissue Targeting

Mary R. Adams[†], **Christopher T. Moody**[†], **Jennifer L. Sollinger**[†], **Yevgeny Brudno**[*,†,‡]

[†]Joint Department of Biomedical Engineering, University of North Carolina, Chapel Hill and North Carolina State University, Raleigh. 911 Oval Drive, Raleigh, North Carolina 27695, United States

[‡]Lineberger Comprehensive Cancer Center, University of North Carolina, Chapel Hill, 450 West Dr., Chapel Hill, North Carolina 27599, United States

Abstract

Local presentation of cancer drugs by injectable drug-eluting depots reduces systemic side effects and improves efficacy. However, local depots deplete their drug stores and are difficult to introduce into stiff tissues, or organs, such as the brain, that cannot accommodate increased pressure. We present a method for introducing targetable depots through injection of activated ester molecules into target tissues that react with and anchor themselves to the local extracellular matrix (ECM) and subsequently capture systemically administered small molecules through bioorthogonal click chemistry. A computational model of tissue-anchoring depot formation and distribution was verified by histological analysis and confocal imaging of cleared tissues. ECM-anchored click groups do not elicit any noticeable local or systemic toxicity or immune response and specifically capture systemically circulating molecules at intradermal, intratumoral, and intracranial sites for multiple months. Taken together, ECM anchoring of click chemistry motifs is a promising approach to specific targeting of both small and large therapeutics, enabling repeated local presentation for cancer therapy and other diseases.

Keywords

drug delivery; click chemistry; pancreatic cancer; brain delivery; extracellular matrix; computer modeling

[*]**Corresponding Author** ybrudno@ncsu.edu.

The authors declare no competing financial interest.

ASSOCIATED CONTENT

Supporting Information

The Supporting Information is available free of charge at https://pubs.acs.org/doi/10.1021/acs.molpharmaceut.9b00589.

Step function and mesh geometry for the COMSOL model, COSMOL material parameters, images and quantitation of NHS-ester distribution in tumors, details on histopathology experiments for immunocompatibility of azide-sNHS esters, full IVIS images for data shown and quantified in the paper, calibration curve used to quantify the percentage of administered dose captured, IVIS images of excised tumors, and UV–vis of antibody-DBCO conjugates (PDF)

INTRODUCTION

Predictable, sustained, and perpetual drug presentation exclusively at disease tissues would be transformative for medicine. This therapy would have four components: (1) drug presentation would be exclusively local, without systemic side effects; (2) drugs could be maintained at disease sites indefinitely, without invasive procedures or avenue for infection; (3) drugs could be administered as needed, providing temporal regulation over drug presentation; and (4) the drug or dose could be changed in response to disease progression or observed local toxicity. Toward this goal, previous efforts reported refillable depots, injectable, drug-eluting hydrogels capable of capturing prodrugged refills from the circulation.[1,2] Although promising, the injectable depots could not be introduced into stiff tumors or target tissues that cannot accommodate increased pressure, such as the brain. In this report, we present extracellular matrix (ECM) anchoring as an alternative to introduce refillable depots in stiff tumors and in the brain for targeting with small molecules and antibodies.

Local presentation of drugs could alleviate many of the limitations to systemic drug administration in cancer. Toxicity in response to systemic drug administration is a central obstacle in the clinic. In addition to systemic symptoms—nausea, fatigue, and pain—drug dose is often limited by adverse effects on nontarget organs, including cardiotoxicity, nephrotoxicity, anemia, digestive issues, and fatigue.[3] This toxicity causes discomfort and distress to patients and their families and limits treatment tolerability. Even agents generally considered targeted,[4] including kinase inhibitors and receptor antagonists, disrupt the growth of normal cells and can elicit unique organ-specific toxicities.[5,6] Finally, many cancer therapies can even cause secondary tumors.[7]

In addition to reducing systemic toxicity, local drug-eluting depots may overcome challenges in chemotherapy delivery to stiff, ECM-rich tumors. ECM proteins in tumors, including collagen and elastin, help sustain and develop a tumor[8,9] and also prevent chemotherapy from reaching cancer cells. In particular, pancreatic tumor ECM proteins are essential for tumor function, invasion, and proliferation.[10,11] The combination of the higher density of ECM and the alignment of the protein fibers has been shown to protect tumors from systemically administered drugs.[12] The high ECM content in these tumors has motivated the use of antistromal agents in a clinical setting, but these targeted antistromal therapies demonstrate only modest results in the clinic, and pancreatic cancer still has an extremely low five-year survival rate of less than 6%,[10] suggesting that alternative methods are needed to deliver drugs to ECM-rich tumors.

Local drug-eluting depots, such as the brain-implanted carmustine-eluting Gliadel, provide benefits but have several drawbacks. Local presentation of therapeutics can be accomplished by locally eluting drug depots that are implanted at a disease site and offer controlled and tunable drug release, biodegradability, and foreign body response.[13] However, many locally eluting depots rapidly deplete their drug stores, require large volumes, and cannot be refilled, reducing their utility in treating disease. For example, the Gliadel wafer, which is implanted intracranially at glioblastoma brain tumor resection sites or during craniotomy, provides a slow release of chemotherapy to the extracellular fluids of the brain.[14] However,

Gliadel has only modestly increased patient survival likely due to the drug's limited diffusivity into the brain parenchyma, limited amount of drug in the wafer, and possible drug resistance that develops over time.[15] A localized drug-eluting depot that diffuses throughout a disease site and can be refilled multiple times with multiple types of drugs would mitigate current therapeutic limitations and improve patient quality of life.

To fully realize the potential of local cancer therapy, repeated and controlled drug presentation at inaccessible tumor sites, including in the brain, is necessary. Intratumoral injections are a direct way to allow drug presentation in disease site ECM. This strategy has been useful for both chemotherapy[16] and immunotherapy,[17] which have shown regression responses in the clinic. However, one intratumoral injection is often not enough for a curative effect and these therapies are often supplemented with systemic chemotherapy.[18] Although repeated intratumoral injections are possible in accessible tumors such as melanoma and head and neck cancers, they are not feasible for internal tumors, including in internal organs such as the pancreas and in brain cancer. To mitigate this gap in drug delivery, Brudno et al. introduced noninvasive methods to refill drug depots.[1] The system utilizes bioorthogonal click chemistry between azides (Az) and cyclooctynes (CO), which is a fast, highly specific, and biocompatible reaction in vivo.[19,20] In the refillable depot technology, a depot hydrogel conjugated to click chemistry motifs is administered through injection at a disease site and captures systemic molecules carrying the complementary click motif. The unique advantage of this approach is that the refills are formulated as prodrugs that release drugs at tunable, controlled rates.[21] The tuned release of therapeutics ensures that the majority of the prodrug is either caught at the target site and given time to release the drug or cleared from circulation by the time the active drug is released. The combination of refillable local depots and prodrug refills eliminates systemic toxicity[1] but allows local, controlled release of active drugs.

Although refillable depots offer many improvements to nonrefillable drug-eluting depots, they have one major limitation: the hydrogels must be injected at the site of disease, meaning that either the tissue must accommodate the hydrogel injection or a cavity must be formed to accommodate the hydrogel, for instance, through tumor resection. To overcome this limitation, we reasoned that a reactive small molecule click motif could be used to anchor itself to the extracellular matrix of target tissues. The molecule needs to be soluble in saline and diffuse into tissue upon infusion, allowing the click groups to reach deep into the target tissue.

In this study, we present a method to specifically label tumor and tissue ECM to create a disperse tissue depot (Figure 1). We take advantage of *N*-hydroxysuccinimide (NHS)-ester chemistry to anchor extracellular ECM with click capture motifs, allowing for improved tissue coverage. The NHS esters of carboxylic acids are widely used for labeling biological molecules in aqueous media by reacting with primary amines, which exist at the N-terminus proteins as well as at lysine side chains. Primary amines occur predominantly on the outside surfaces of native proteins where they are readily accessible to conjugation reagents introduced into the aqueous medium.

We present a finite element analysis model to predict the reactive diffusion and anchoring of a click depot within target tissues from the depot implantation. We then compare the model to experimental results using a sulfo-*N*-hydroxysuccinimide (sNHS) ester fluorophore in murine tumor and brain tissue. Using the depot establishment information, we demonstrate dibenzocyclooctyne (DBCO) homing efficiency at dermal and tumoral sites and in the brain for both small molecules and antibodies with minimal immune response. Finally, we demonstrate targeted and spatial separation of small molecule depots in vivo utilizing two bioorthogonal chemistries.

MATERIALS AND METHODS

3-Azidopropionoic acid sNHS ester (1083), DBCO-Cy7 (1047), alexa Fluor 488 (AF488) NHS ester (1338), AF647 NHS ester (1344), and methyltetrazine sNHS (1193) were purchased from Click Chemistry Tools (Scottsdale, AZ) as dry desiccate powders and stored at −20 °C. All were dissolved in sterile 0.22 μm filtered 1× phosphate buffered saline (PBS) immediately before use and discarded after being dissolved. DBCO-Cy7 was first dissolved in dimethylsulfoxide (DMSO) and then diluted 1:100 in 1× PBS and consisted of 1% DMSO in the administered intravascular (iv) dose concentration.

For antibody conjugation, the anti-human PD1(CD279), free of the sodium azide preservative, was purchased from BioXcell. DBCO-peg4-NHS (Sigma 764019) was first dissolved in DMSO, followed by dilution with PBS to a concentration of 10 mg/mL. DBCO-sNHS from Lumiprobe was dissolved in PBS at a concentration of 5 mg/mL.

KPC 4662 pancreatic tumor cell vials were received frozen from the laboratory of Dr. Pylayeva-Gupta at UNC at Chapel Hill at passage 9. Cells were thawed and passaged to p12–14 before subcutaneous tumor inoculation in 1:1 PBS/matrigel matrix (lot 7205011). The culture medium was made of 1× high-glucose Dulbecco's modified Eagle's culture medium (DMEM) (Sigma lot RNBG8364), 10% fetal bovine serum (Thermo Fisher Scientific), and 1% 10 000 U/mL penicillin/streptomycin (Thermo Fisher Scientific). For splitting cells, we used 0.05% trypsin–ethylenediaminetetraacetic acid (EDTA) (Thermo Fisher Scientific) to detach cells from T75 flasks.

Brain surgeries required a Viamed #10 scalpel (lot D0167), lidocaine HCL (Alfa Aesar W06D062, lot #W06D062), Visine eye drops, Vet bond tissue glue, and a Braintree scientific ideal microdrill with a 0.25 mm burr. The Kopf 900LS manual stereotaxic setup with a UMP3 microinjector (World Precision Instruments) was used to control injection speed into the brain coordinates and attach a 5 μL (65460–03 Neuros lot #595070) Hamilton syringe. A Kopf 701 anesthesia mask attachment was also used to provide continuous isoflurane to the mouse undergoing intracranial procedures. Perfusion of animals was performed with sterile PBS and 10% formaldehyde solution from MACRON diluted to 4% in PBS with an Automate In Vivo Manual Gravity Perfusion System (Braintree Scientific) through a 27g needle.

For clearing using the iDisco protocol, methanol (Acros organics B0533672), dichloromethane (DCM) (270997 Sigma), and dibenzyl ether (DBE) (Sigma BCBT7116) were used.

Conjugation of PD1 antibody to cyanine 7 (Cy7) and DBCO: Anti-human PD1 antibody; 0.4 mg of the antibody was left to react at room temperature for 1 h with 8 equiv of DBCO-peg4-NHS ester and Cy7-sNHS ester. The mixture was filtered with a 10 K amicon filter (Thermo Fisher Scientific) and spun 3× at 12 000*g* for 10 min to remove unreacted NHS esters. A control solution without the antibody was used to verify filtering efficiency. The concentration of the conjugated antibody and the amount of the conjugated fluorophore and DBCO were verified by nanodrop UV/vis spectroscopy.

Computational Depot Modeling Using COMSOL Multiphysics.

COMSOL 5.4a Multiphysics finite element analysis software was used as the platform to model azide-sNHS ester diffusion and reaction within a tumor extracellular space (Figure 2A,B). A zero-dimensional (0D) time-dependent chemical reaction engineering model solved for the NHS-ester chemistry kinetics in a semibatch reactor setting based on the expected reaction rates and the number of amines available to react with over time in the disease site.

The 0D component consists of two irreversible competing reactions with the aminolyzed species treated as a surface reaction and the hydrolyzed species as a solvent. This was solved in a time-dependent model for 10 000 s. A parameter sweep was used to verify the solution with varying different reaction rates.

The 0D time-dependent chemical reaction was layered on a two-dimensional (2D) axisymmetric space-dependent model to incorporate the geometry of a tumor, flux of injection from the needle source, and reactive porous media flow throughout a tumor extracellular matrix. The geometry was created using a 500 mm^3 tumor as a reference, the shape of which we estimated as a sphere with a radius of 4.923 mm and the inner 27g needle injection creating a radius sphere of 0.205 mm. The flux of injection out of a 0.205 mm sphere in the middle of the tumor was directed outward along the circumference of the inner sphere at a rate to deliver 10 μmol of azide-sNHS ester in 50 μL over the first 500 s of the model to match the experimental infusion rate conditions. The outside circle circumference flux was set to atmospheric gauge pressure at the start of the simulation. The diffusivity of the azide-sNHS ester molecule with MW = 314 was estimated to be similar to that of sucrose (MW = 343, 5×10^9 m^2/s) in the tumor.[22] The dynamic viscosity of 300 Pa s,[23] porosity of 0.2,[24] and permeability of 1×10^{-17} m^2 for the tumor[25] were obtained from the literature. Tissue properties such as electrical conductivity and heat capacity were assumed to be similar to those of water at body temperature.

The 2D model was solved in two steps. First, a stationary model solved for Darcy's law of fluid flow, considering the flux of the injection to set up a force to move the diluted species through the tumor material area. Next, a time-dependent model solved for the porous media flow and reaction engineering kinetics to give a space-dependent and time-dependent output. The mesh was extra fine tetrahedron shaped and is shown in Supporting Figures 1 and 2 and

Supporting Tables 1 and 2. Figure 2C and Supporting Figure 3 are a direct output from the COMSOL results section, while Figure 2D shows the integration of the extracted results over the entire simulation time at individual radial coordinates to obtain the total amount of anchored azide per radial coordinate over the entire simulation time.

Imaging of Depot Anchoring to the Tumor ECM.

To characterize the co-localization of collagen and AF647 NHS, approximately 1 million p12 KPC 4662 murine pancreatic tumor cells in 1:1 PBS/matrigel were inoculated subcutaneously on the dorsal flanks of female C57BL/6J mice. On day 12 after KPC 4662 pancreatic tumor injections, 50 μL of 0.2 mM AF647 NHS ester ($n = 2$) was infused intratumorally. All of the tumors were at least 150 mm^3 in volume, and the 50 μL volume was delivered over 1 min with a 27g winged catheter and retracted over an additional minute slowly. One day after intratumoral NHS infusion, mice were perfused by intra-arterial infusion of 20 mL cold PBS followed by 20 mL of 4% formaldehyde through a 27g winged needle infusion set and tumors were extracted. The tumors were fixed in 4% formaldehyde, rinsed, and cryoprotected using 30% sucrose in PBS. Tumors were embedded in optimal cutting temperature compound (OCT) (Fisher Healthcare, #4585) and cryosectioned at 10 μm. Slides were rinsed in distilled water and then incubated in 0.1% picrosirius red solution for 30 min at room temperature. Slides were then dehydrated using two changes of absolute alcohol, cleared in xylenes, and cover-slipped using DPX (Electron Microscopy Sciences, #13512).

Alexa Fluor 488 Depot Histology Methods.

Approximately 750k p12 KPC 4662 murine pancreatic tumor cells in 1:1 PBS/matrigel were inoculated subcutaneously on the dorsal flanks of female C57BL/6J mice. On day 9 after KPC 4662 pancreatic tumor injections, 50 μL of 5 mM AF488 NHS ester ($n = 3$) or PBS as control ($n = 3$) was infused intratumorally. All of the tumors were at least 150 mm^3 in volume, and the 50 μL volume was delivered over 10 min with a 27g winged catheter attached to a syringe pump. One day after intratumoral AF488 infusion, mice were perfused by intra-arterial infusion of 10 mL cold PBS followed by 4% formaldehyde through a 27g winged needle infusion set and tumors were extracted.

For intracranial injections, healthy outbred CD1 mice were infused with 2 μL of 5 mM AF488-sNHS ($n = 3$) or PBS ($n = 3$) as a control into the right brain hemisphere over 10 min with a 27g winged catheter attached to a syringe pump and perfused 5 days after infusion. Perfusion was performed by intra-arterial infusion of 10 mL cold PBS followed by 4% formaldehyde through a 27g winged needle infusion set, and the brains were extracted.

The iDisco protocol was followed[26] for the extracted tumors and brains. Tumors and brain samples were removed from perfused animals and fixed in 4% formaldehyde for 24–48 h. The tissues were shaken at room temperature in increasing concentrations of methanol (20, 40, 60, 80, 100, 100, and 100%) for 1 h each. Once the sample was fully dehydrated, the tissue was shaken in three rounds of DCM for 30 min, and finally, the optical properties of the tissue were changed when the samples were placed in DBE. Cleared samples were imaged on a Lavision Ultramicroscope II and evaluated on IMARIS version 9. The samples

were imaged at 7 μm increments in the *z* direction with 40% laser power on the 488 nm wavelength. The width of the light sheet was set to 100% to visualize the entire sample; NA was set to 21 μm, 0.63× zoom, and focus-adjusted so that lasers illuminated both sides of the sample. Postprocessing included creating isosurfaces for the 488 nm signal, and signal threshold values were further lowered to create a surface for the entire tissue volume incorporating natural tissue autofluorescence at the 488 nm wavelength. The entire tissue was set to be a white color surface with 80% transparency, and the 488 signal volume was made into a green surface. Analysis in the software included volume statistics of the isosurfaces made as well as isoplanes to find the widest distance of the detectable signal in each tissue measured. The IMARIS software allows for a natural detection of high levels of 488 nm signal and automatic differentiation of 488 nm signal from the natural tissue fluorescence. The values for radial diffusion from the injection site were found by finding the cross section of the intratumor signal with the widest diameter of the signal, divided by 2 to get a radius and further by 0.8 to account for shrinking during the iDisco process. A shrink factor of 0.8 was found from averaging caliper measurements before the protocol was followed (samples in formaldehyde) and after imaging on the microscope.

Targeting of Intradermal Depot.

Female CD1 mice (Envigo, 8 week old) were injected intradermally with 50 μL of 0.1 M azide-sNHS in PBS ($n = 4$) or PBS as control ($n = 4$) and imaged on the IVIS imager to obtain a background fluorescence signal. IVIS excitation wavelength was indocyanine green (ICG) BKG and emission wavelength ICG for all IVIS images presented with no image math in the IVIS software performed. For IVIS images, only radiant efficiency values were used to normalize the data over variable exposure times. All mice were then retro-orbitally injected with 100 μL of 50 mg/L DBCO-Cy7, followed by IVIS imaging at 5 min, 1 h, and 24 h. The increase in radiant efficiency measured was found by subtracting the region of interest (ROI) values before the DBCO-Cy7 injection from the 24 h after imaging. The procedure was repeated at 30, 90, and 180 days.

To characterize the immune response to azide-sNHS, 8 week old CD1 mice from Envigo were injected intradermally with 50 μL of azide-sNHS (0.1 M, $n = 4$) or PBS ($n = 4$) as control. These mice did not receive fluorophore but were sacrificed 1 month later to have the skin at the injection site and main organs (heart, liver, kidneys, lungs, and spleen) embedded in paraffin, sectioned, and stained with H&E by NC State College of Veterinary Medicine's histology core to evaluate immune response to the small molecule. The sections were sent to a certified pathologist for evaluation.

For dual targeting of DBCO to azide and *trans*-cyclooctene (TCO) to methyltetrazine, CD1 mice were injected intradermally with 50 μL of methyltetrazine sNHS (0.05 M) in the right flank and azide-sNHS (0.05 M) in the left ($n = 4$). Control CD1 mice ($n = 4$) were injected with 50 μL of PBS on both sides intradermally. All mice were then imaged for a before background fluorescence picture and then retro-orbitally injected with 100 μL in both eyes of a mixed solution containing equal amounts of DBCO-Cy7 and TCO-Cy5 at a 50 mg/L concentration. Mice were imaged on IVIS 48 h after iv injection. Cy7 was imaged using

ICG BKG excitation and ICG emission filters. Cy5 was imaged using Cy5.5 BKG excitation and Cy5.5 emission filters.

Targeting of Intratumoral Depots with Cy7-DBCO.

Approximately 750 000 p12 KPC 4662 murine pancreatic tumor cells in 1:1 PBS/matrigel were inoculated subcutaneously on the dorsal flanks of albino female C57B/6 8 week old mice from Envigo. The mice were infused intratumorally with 50 μL (0.2 M) of azide-sNHS ester in PBS ($n = 4$) or PBS as control ($n = 4$) over 10 min through a 27G winged catheter attached to a syringe pump (Harvard Apparatus 70–4500), and images were taken on the IVIS spectrum imager. On day 9 following tumor inoculation, mice were retro-orbitally injected with 100 μL of 50 mg/L DBCO-Cy7 and imaged 24 h after iv injection. iv injection and imaging were repeated at 12 and 15 days postinoculation. Cy7 was imaged using ICG BKG excitation and ICG emission filters.

Targeting of Intratumoral Depots with PD1 Antibody-Cy7-DBCO.

Approximately 750 000 p12 KPC 4662 murine pancreatic tumor cells in 1:1 PBS/matrigel were inoculated subcutaneously on the dorsal flanks of 8 week old albino female C57B/6 mice from Envigo. The mice were infused intratumorally with 50 μL (0.2 M) of azide-sNHS ester in PBS ($n = 4$) or PBS as control ($n = 4$) over 10 min through a 27G winged catheter attached to a syringe pump (Harvard Apparatus 70–4500), and images were taken on the IVIS spectrum imager. On day 9 following tumor inoculation, mice were retro-orbitally injected with 100 μL of 3.2 μmol/mL PD1 antibody-Cy7-DBCO and imaged 24 h after iv injection.

Targeting of Intracranial Depots.

Female CD1 mice (12-week old) from Charles River laboratories were used. For anesthesia, surgeries had 1–5% isoflurane before procedures as well as continuously through the stereotaxic setup in a Kopf 701 anesthesia mask. Mice were mounted on a Kopf stereotaxic head stage using ear bars, and the 5 μL Hamilton syringe with a 33g removable needle was placed in the microinjector attachment (World Precision Instruments UMP3 system) mounted on the stereotaxic frame. For surgery, the area on the head was shaved and washed with 70% alcohol and chlorhexidine solution using cotton-tipped applicators. Lidocaine HCL (100 μL, 5 mg/mL) was injected subcutaneously above the skull through a 27-gauge insulin syringe for pain relief during surgery. An incision with a #10 scalpel was made from posterior to anterior (the start of the skull to between eyes), and the skin was pulled away from incision using sterile Q-tips to expose the skull. The syringe needle was adjusted so that the tip of the needle landed on Bregma (the position of the stereotaxic device was recorded) and then moved to the desired calculated position where a mark was made with a sterile surgical marker (1 mm anterior, 2 mm laterally right, and 2.5 mm deep with respect to Bregma). A microdrill made a 1–2 mm size hole in the skull for the injection needle. Once the hole was wide enough, the needle was adjusted to the injection position and slowly lowered to a desired depth from the skull opening. Azide-sNHS (2 μL, 0.2 M) in PBS ($n = 4$) or PBS as control ($n = 4$) was injected using a microinjector at a flow rate of 3.3 nL/s over 10 min. Once complete, the needle was left in place for 3 min and pulled up slowly over the next 5 min until out of the mouse completely. The incisions were glued with Vet bond, and

the animals were placed in a heated recovery area until ambulatory. Each mouse was then left to heal for three weeks before imaging and fluorophore targeting experiments. Fluorophore injections were performed as described for previous imaging techniques, except the administration was done through the tail vein to minimize the background signal, sometimes seen with retro-orbital injections, in the head area.

Statistical Analysis.

All significant differences presented in this paper were found by Student's *t*-test statistics in Prism software and noted in figures as $*p < 0.05$, $**p < 0.01$, and $***p < 0.001$.

RESULTS

Computational Modeling of ECM Decoration by *N*-Hydroxysuccinimide Esters at Pancreatic Tumor and Intracranial Sites.

We reasoned that activated sNHS esters injected locally could react with the proteins of the extracellular matrix to anchor capturing click groups to tissue ECM. To better understand the diffusion and anchoring of the click groups, we created a computational model of the reaction kinetics. COMSOL Multiphysics was used to model the reaction behavior and location of the azide-linked NHS esters using the parameters presented in Figure 2A. Injected NHS esters have one of the two fates, corresponding to two competing reactions: either the NHS ester reacts with amines in the ECM or the NHS ester is hydrolyzed by water and inactivated. The rates of aminolysis and hydrolysis of NHS esters were based on literature values: 1.02×10^{-3} [1/s] (aminolysis) and 4.5×10^{-5} [1/s] (hydrolysis) at physiological pH.[27–29]

To enable informed and physiologically relevant modeling, it was necessary to estimate the concentration of amines available for the reaction with NHS esters in target tissues. Primary amines available within ECM were estimated through published quantities of collagen-1, multiplied by the amount of lysines per collagen strand. For pancreatic tumors, collagen contents of 54.72 μg/mg of wet tissue have been reported, and with 58 lysines per collagen chain, this translates to roughly 22 mmol of amines per liter of pancreatic tumor.[30] We used this quantity to solve the reaction kinetics, which was further layered on the 3D reactive flow model.

From a 0D semibatch reactor setup in COMSOL, we found that approximately 80% of the injected azide-sNHS molecule will react with primary lysines in the extracellular matrix (Figure 2C). The chemical reaction kinetics was layered on a 2D axisymmetric reactive flow model. The flow migrated throughout the tumor by the force of the needle infusion needle flow (Supporting Figures 3 and 4). The entire reaction is predicted to be complete within 15 min after the start of the needle infusion. Figure 2D and Supporting Figure 5 show the integrated amount of anchored azides over radial coordinates from the infusion needle from a 50 μL infusion of azide-sNHS in saline. The model predicts a sphere 6–7 mm in diameter with decreasing anchored azide concentration farther from the infusion hole. The COMSOL model predicts that approximately 5 μmol decoration is achieved directly surrounding the infusion needle, with a slow decrease in concentration with increasing distance. These

results predict that the majority of sNHS molecules react with surrounding ECM within 7 mm of the infusing needle for a 50 μL injection into stiff, pancreatic tumors.

Imaging of Depot Anchoring to the Tumor ECM.—To test the predictions of the computational model empirically and visualize the formation and distribution of ECM-anchored depots within and around a disease site, we injected fluorescent NHS-ester molecules locally into pancreatic tumors. We chose pancreatic tumors specifically due to their high stiffness and fibrosity,[11] which makes intratumoral injection of conventional hydrogel depots difficult. In contrast, the collagen-rich environment means that reactive NHS esters can take full advantage of ECM anchoring.

To assess both NHS-ester retention and distribution through the tumor, a model fluorescent NHS ester (Alexa Fluor 647 NHS) was infused intratumorally. To quantify the percentage of injected NHS ester anchored to insoluble ECM, mice were imaged directly after injection and 24 h after injection. Approximately 60% of the signal remained in the tumor after 24 h (Supporting Table 3), suggesting that 40% was lost through a combination of hydrolysis and reaction with soluble factors. After the 24 h stabilization, tumors were excised, fixed, and sectioned and counterstained for extracellular protein with picrosirius red. Figure 3 shows that the AF647 signal strongly co-localized with the picrosirius signal, confirming the hypothesis that AF647 reacts with proteins in the ECM.

To assess NHS-ester distribution throughout the tumor in three dimensions, tumors were submitted to tissue clearing and confocal imaging. A fluorescent NHS ester (Alexa Fluor 488 NHS) was infused intratumorally and left to stabilize for 24 h followed by animal perfusion and tumor excision. Tumors were surgically removed from mice and submitted to tissue clearing using the iDisco clearing protocol.[25,26,31] The entire tumors were imaged via light sheet microscopy and postprocessing in IMARIS software. Volumetric representations of the whole tumor sample area distinct from just the AF488 NHS signal were created. The process and results are shown in Supporting Figure 6. For each tumor, volumetric isosurfaces allowed evaluation of both the tumor volume and NHS fluorophore signal. Two of the tumors had signal preferentially coating on one side of the tumor, while one of the samples had a sporadic signal in all directions from the center infusion needle. From the isosurfaces in IMARIS, we estimate that approximately a quarter of the 50 μL injection volume was easily observed at the tumor, while the remainder is likely to have anchored to surrounding areas around the tumor. The IMARIS isosurfaces showed a strong fluorescent signal approximately 5 mm radially from the middle of the tumor, in good agreement with estimates from the COMSOL simulation (Table 1). A strong fluorescence signal was observed on the outside of the tumor. We hypothesize that the fibrous capsule around the tumor stopped flow outward and acted as a substrate for covalent binding of the NHS ester. Taking out more tissue from around the tumor or other imaging techniques might improve this characterization.

Imaging of Depot Anchoring to the Brain ECM.—To evaluate the predictions of the COMSOL models and visualize the formation and distribution of ECM-anchored molecules after intracranial injections, we assessed the tissue penetration of a model, fluorescent NHS ester injected locally into healthy brains. It was reasoned that unlike injections of viscous or

implantable hydrogel depots, injection of NHS molecules could be performed without creating substantial intracranial pressure. Alexa Fluor 488 NHS ester was infused into the brain (0.2 M, 2 μL). After five days, mice were euthanized by perfusion and brains were removed and submitted to clearing using the iDisco clearing protocol. Whole-brain imaging using light sheet microscopy and postprocessing in IMARIS software allowed volumetric representations of the whole brain as well as the AF488 NHS signal. Imaging results demonstrate that the entire 2 μL of AF488 NHS infusion remained in the striatum area at the injection site. In all three samples, the diffusion in any direction was limited to 1–2 mm in the striatum (Figure 4). A small amount of needle track backflow was observed in the cranial/rostral direction.

Isosurface representation allows a reasonable estimate of the distribution and distance of the infused small molecule, which was in good agreement with the COMSOL model. All three brain injections visually looked similar with slight variations coming from individual injection variability.

Noninvasive Targeting of ECM-Anchored Click Groups.—A critical aspect to enable therapeutic targeting of ECM-anchored molecules is the in vivo targeting of systemically circulating molecules that can be captured on the depot site. Previously, we and others have demonstrated that cyclooctyne-conjugated molecules efficiently target azide depots; thus, we tested whether ECM-anchored azide molecules could efficiently capture circulating cyclooctynes. To anchor azides to tissue ECM, we chose sulfo-NHS (sNHS) esters of azide due to its superior solubility in saline. The maximum solubility of the azide-sNHS ester in PBS was found to be 0.2 M and was used in all targeting experiments unless otherwise stated. Healthy CD1 mice were injected intradermally and did not exhibit any noticeable skin irritation, redness, or swelling in the following 180 days. Intradermally anchored azides demonstrated efficient capture of iv-injected fluorescent cyclooctynes 30, 90, and 180 days after intradermal injection (Figure 5A,B). Imaging of the mice in the first 24 h after iv provided insights into DBCO-conjugated fluorophore capture at the intradermal azide depot site with strong systemic fluorescence in the first few minutes and hours after iv injection, but the fluorophore concentrated at the site of injection by 24 h after iv administration (Figure 5C). With repeated systematic dosing, we were able to see the depot capture fluorescent DBCO molecules from circulation up to 6 months after intradermal depot injection. However, attempts to demonstrate capture 8 months after intradermal injection were not successful.

Previous work has suggested that in addition to the azide-CO chemistry, tetrazine-trans cyclooctene (Tz-TCO) chemistry is promising for in vivo targeting.[19,31–34] To test the compatibility of this chemistry together with azide-cyclooctyne and show potential spatial separation of the two distinct click chemistries, the two chemistry pairs were tested in the same animal. Azide-sNHS and methyltetrazine sNHS were injected at two intradermal sites on the animal, with the concentration of the azide-sNHS lowered to match the solubility limit of methyltetrazine sNHS (50 μL, 0.05 M). A 1:1 mix of TCO-Cy5 and DBCO-Cy7 was administered iv, and mice were imaged 24 h after iv injection. The methyltetrazine sNHS-(blue) signal appeared to have a wider diffusion radius than azide-sNHS(red). Efficient and selective targeting by the two small molecules to their respective depot sites was observed

(Figure 5D) with about 0.5% of administered dose localizing to this site (Supporting Figures 9 and 10, Table 4).

To study both the local and systemic toxicity or local immune response to intradermally injected ECM-anchoring azides, immunocompetent, outbred CD1 mice were injected intradermally (0.1 M, 50 μL). No redness or swelling was observed at the injection site at any point. One month after intradermal injection, Hematoxylin and Eosin-stained sections of the injection site as well as the heart, lungs, spleen, kidneys, and liver were evaluated by a licensed pathologist (Figure 5E; see Supporting Table 4 and pathologist's notes). Neither the azide-sNHS-injected skin nor any of the major organs were deemed different from PBS-injected controls, and no foreign body response was observed to the depot, suggesting that this technology may be suitable for both cancerous and noncancerous applications.

Noninvasive Targeting of ECM-Anchored Click Groups at Tumor Sites.—Having demonstrated efficient click-enabled targeting of intradermal sites, we tested whether the same method could be used to target small molecules and antibodies to pancreatic tumors. We reasoned that ECM anchoring would be particularly useful for cancers that have large amounts of ECM, such as pancreatic tumors.[35] First, the relative captured dose at the tumor was quantified. Intratumoral injections of azide-sNHS were followed by iv administration of DBCO-Cy7, and the captured dose was assessed by in vivo imaging. Capture of DBCO-Cy7 at tumors receiving azide-sNHS exceeded PBS-injected controls by fourfold (Figure 6A–C and Supporting Figures 11–16). To quantitatively assess the percent of administered dose captured at the tumor, the fluorescence signal of tumors was compared to a linear calibration curve of the fluorophore signal. In contrast to subcutaneous depots, which captured between 0.5 and 1% of the administered dose (Supporting Table 5), we measured that approximately 7.8% of the administered dose was present in the azide-sNHS-injected tumors (Supporting Figures 15 and 16) compared to 2.22% in the PBS-injected tumors at 24 h after iv administration.

Next, we evaluated the ability of ECM-anchored azides to repeatedly capture DBCO-Cy7 while the tumor continued to grow. Our data proves that there are still active azide sites available through systemic circulation for three iv administrations in tumor ECM. Further targeting experiments were not possible due to the fast rate of tumor growth in the KPC 4662 model that necessitates euthanasia by day 18. Figure 6B also shows that the fluorescence of the targeting is decreasing slightly, but it is suspected that this is due to tumor growth obstructing fluorophore radiance, rather than molecule capture.

It was next evaluated whether a therapeutically relevant antibody could also be specifically captured at an intratumoral depot site. An anti-human PD1 antibody was conjugated to both DBCO and Cy7 (Supporting Figure 17). Mice carrying KPC 4662 pancreatic tumor were intratumorally injected with azide-sNHS or PBS and then iv administered Cy7- and DBCO-conjugated anti-human PD1 antibody. After 24 h of iv administration, mice were imaged on IVIS (Supporting Figure 18) and then euthanized, and tumors were extracted and further imaged. Figure 6D shows the extracted tumors, and Figure 6E shows the quantification of fluorescence in the tumors, demonstrating a statistically significant difference between azide-sNHS and PBS-treated animals.

Taken together, our data proves that intratumorally anchored azide motifs can repeatedly and efficiently capture systemic small molecules and antibodies.

Noninvasive Targeting of ECM-Anchored Click Groups at Intracranial Sites.— In addition to stiff, fibrous tumors, ECM anchoring could prove useful at intracranial sites, where injection of viscous materials or implantation of hydrogel depots might prove difficult. To assess the capture of DBCO-conjugated small molecules at the intracranial location, 2 μL of azide-sNHS (or PBS control) was injected intracranially and mice were allowed to heal for 21 days to allow for glial scar formation from the cerebral injection.[36] A glial scar is formed in reaction to the central nervous system trauma and consists of ECM molecules, which form stiffer scar tissues around affected areas, and upregulated vimentin, collagen 4, laminin, and glial fibrillary acidic protein (GFAP).[36] This delay also allowed for most of the cranial incision skin wounds to be healed, but notably some were not completely closed up on all of the mice at the first iv administration. In the first iv DBCO-Cy7 administration, no significant differences between azide-sNHS and PBS groups were observed. This could have been because not all of the head wounds were completely closed, the variability of accessible azide binding sites, and possible iv injection variability. By the end of 1 month, at the second administration time point, significant differences were observed in fluorophore capture in the azide-sNHS-injected mice as compared to PBS control. The third iv administration, on day 40, also showed efficient and specific capture of iv DBCO-Cy7 as compared to negative control (Figure 7C and Supporting Figures 18–20)

DISCUSSION

This paper reports the creation of targetable depots in tissues by anchoring click chemistry motifs to the extracellular matrix. The anchoring of click motifs to the ECM was modeled using a computational finite element analysis model to understand NHS-ester infusion, tissue diffusion, and reaction with the ECM within diseased and healthy tissues. This model was then validated through injection and imaging of model fluorescent NHS molecules in tumors as well as in the brain to obtain in vivo visualizations of depots. It was demonstrated that click chemistry groups could be anchored at tumor tissues and could efficiently and specifically capture fluorescent click partners from the circulation at intradermal sites, within the fibrous matrix of pancreatic tumors and in the brain. The depot was nontoxic and nonimmunogenic and persisted for up to 6 months. Taken together, this system is a promising approach to decorating disease tissues for targeting with click-conjugated therapeutics, including small molecules, biological agents, and antibodies.

The computational model of NHS reaction kinetics provides insights into tissue diffusion of NHS esters. As with any model, certain limitations persist. First, the model incorporates only fluid flow and the reaction of the azide-sNHS ester with amines or with water. We reason that the reaction kinetics and flow rate are the most critical parameters in establishing the tissue depots but realize that mechanical and thermal properties also play a significant role in vivo. The density of tumors and placement of the infusion needle are all additional complications to the model. The diffusion parameters for this molecule were based on estimated values for similar molecules in the literature, as this particular molecule has not been studied in this manner. Additionally, pH in the tumor microenvironment has been

reported to be more acidic than the 7.4 used in the model parameters, so the values used may be an underestimation of the reactive azides available as both aminolysis kinetics and hydrolysis reaction kinetics decrease at lower pH. An additional complication is the unpredictable and heterogeneous nature of tumors due to necrosis or blood pooling “cracks”, which cause abnormal ECM and may form pathways for infused substances to travel through the tumor.[37] Future modeling will introduce flow through the lymphatic pathways in tissues[38] and will model blockage of lymphatics in tumors.[39] Despite these limitations, the computational model allows for the optimization of multiple infusion parameters, NHS-ester dose, concentration, and volume as well as allows modeling of activated esters with alternative aminolysis kinetics, including 4-sulfotetrafluorophenyl (STP),[40] HNSA,[41] and acyl chlorides. Thus, we have found the computational model to be very useful for the exploration and optimization of infusion parameters before the necessary validation of candidate protocols in vivo.

The computational model also provides useful insights into the anchoring of click groups, which were validated in vivo, in the brain. Factors that might influence this model include the amount of amine binding sites in the brain area of interest, the fluid dynamics in relation to blood vessels and ventricles, and changes in ECM content and concentration in response to disease. Additionally, the glymphatic system, the main drainage mechanism in the brain, might act differently from peripheral lymphatics.[38] The significant difference in brain organization and make-up between rodents and humans will play an important role in model design. Ultimately, the quantity of each brain region, or disease area, will have to be measured and averaged across a wide range of preclinical models to have a full understanding of depot establishment in vivo.

One simplification of the computational model of ECM decoration with sNHS molecules is that it does not include potential reaction with soluble proteins in the extracellular space. Soluble proteins make up a portion of the total protein content of the extracellular space and reaction with these proteins would be predicted to be unproductive for ECM anchoring. The observed retention of roughly 60% of the signal after 24 h suggests that the majority of injected azide molecules are anchored to insoluble proteins. Future studies will focus on the quantitation of this component for a more representative computational model.

One advantage of NHS-ester-mediated depot formation is that unlike viscous gels or implants, these small reactive molecules diffuse into tissues before anchoring. Analysis of the distribution of aminolated fluorescent NHS esters within both tumors and the brain showed good agreement with the COMSOL computational model in terms of spread, but the model failed to predict the heterogeneity of tumor injection. In the tumor, the depot was simultaneously spread widely but also missing from significant portions of the tumor mass. Future work will focus on the development of intratumoral infusion methods that more readily spread out within the tumor, including the possibility of more stable activated esters and more controlled infusion rates.

The efficient, local capture of small molecule fluorophores at dermal, tumoral, and cranial sites after iv administration proves that this depot system can be established in the intradermal skin layer, within a tumor, and in a healthy brain. These distinct injectable drug-

eluting depots can now be captured from the blood with complimentary click motif fluorophores. The use of different chemistries for differential spatial separation of two small molecules that were injected together could be used for targeting of mutually incompatible therapies to different parts of the body for localized activity at disease sites. Further characterization and optimization of how injection concentration and dose affect molecule capture will illuminate depot activity. Ultimately, the reaction rates, stability of the depot, and immunogenicity will all need to be evaluated for each disease state to fully benefit from the proposed therapeutic mechanism. In addition, tissue vascularity will play an important role in the efficiency of device refilling. It is suspected that the difference between homing efficiency in subcutaneous (0.5–1%) versus the tumor (~8%) site may be explained by the difference in the vascularization of these tissues.

An important consideration for the wider deployment of this technique will be the persistence and distribution of azide molecules within the extracellular matrix. We suspect that the more accessible azide groups will be labeled first, followed by a lower-efficiency labeling of less-accessible sites. In addition, matrix turnover over time will lead to a slow elimination of azide groups from the tissue and slow biodegradation of the depot site. Future work will explore the rates and distribution of these processes.

Degradation and efficiency losses may explain the failure to capture circulating DBCO-Cy7 at intradermal sites at 8 months after a successful refilling at 6 months, which was surprising. It is possible that the loss of refilling capacity was due to the lack of accessible azide molecules. Given that 10 μmol of sNHS azide molecules were injected into the tissue and 4 μmol of DBCO-Cy7 were injected into the circulation, we anticipated a theoretical limit of ~25 refills (assuming ~10% capture). Injecting higher volumes or higher concentrations of azide-sNHS could potentially mitigate this issue and is the basis of future work in this area.

One surprising outcome of this research was the efficient intracranial targeting of DBCO-Cy7 in the absence of blood brain barrier (BBB) disruption. The DBCO-Cy7 molecule has a molecular weight of 1250 Da, four anionic sulfate motifs, and numerous hydrogen bond donors/acceptors and, thus, was not expected to readily cross the blood brain barrier.[42] In unpublished data, we showed no significant difference between azide-sNHS-injected mice that received iv mannitol to osmotically open the BBB and azide-sNHS-injected mice without the BBB opening. Because the DBCO molecule is hydrophobic, it is possible that DBCO-Cy7 might transport through the BBB through the transcellular lipophilic pathway or might be fortuitously a poor substrate for efflux pumps. Alternatively, wounding at the site as a result of intracranial injection might allow fluorophore access to the intracranial depot, although the ability to target intracranial depots at 32 and 43 days after intracranial injection makes this possibility less likely. Future work will investigate the precise location of fluorophore binding as well as the macroscopic and microscopic effects that ECM anchoring causes within the brain.

Targeting of intracranial depots with DBCO-Cy7 at 21 days (the first time point in Figure 7C) was unsuccessful. One possibility for this is the formation of a glial scar formed in reaction to the central nervous system trauma, consisting of ECM molecules that form stiffer

scar tissues around affected areas, upregulated vimentin, collagen 4, laminin, and GFAP and preventing circulating molecules from entering the area. We suspect that between days 21 and 28 this scar is fully resolved, allowing small molecule extravasation and depot targeting from the circulation.

The proposed approach provides a versatile method to target a large variety of therapeutics to local tissues. In previous literature, we and others have used click chemistry to selectively localize prodrugged refills to tissues and tumors.[1,2,17,43–45] Slow release of drugs from the click groups afforded sustained release of drugs at target tissues. The ability to locally concentrate molecules following systemic administration would give clinicians temporal control over the course of treatment and allow for using different chemotherapeutic or immunotherapeutic interventions over time. This targeting would also allow clinicians to adopt or change the drug or drug dose to respond to disease progression.

Taken together, this technology demonstrates promise for local, chronic conditions that would benefit from repeated, local, and sustained presentation of therapeutics. The proposed system as a localized cancer treatment is expected to lead to a better quality of life for patients by reducing the drug presentation at nontarget parts of the body as well as appeal to patients because of the relatively noninvasive refilling procedure. The refillable click NHS-ester system as a localized drug depot platform has shown promising results in vivo and calls for further research into its therapeutic efficacy utilizing chemotherapeutic or immunotherapeutic conjugated click molecules.

Supplementary Material

Refer to Web version on PubMed Central for supplementary material.

ACKNOWLEDGMENTS

We would like to thank Justin Park for assistance with tissue clearance and the NCSU CVM staff for proper care of animals used in experiments and valuable resources on training. We would like to thank Dr. Michael Danielle for training and assistance with COMSOL and the COMSOL support staff for help with model troubleshooting. We would also like to thank J. Ashley Ezzell of the Histology Research Core Facility at the Department of Cell Biology, Mariusz Zareba of the Cellular and Molecular Imaging Facility. We are grateful to Dr. Pylayeva-Gupta for the KPC 4662 tumor cells.

Funding

This project was supported by the National Center for Advancing Translational Sciences (NCATS); National Institutes of Health, through Grant Award Number UL1TR002489; the UNC Lineberger Comprehensive Cancer Center’s University Cancer Research Fund; and start-up funds from the University of North Carolina and North Carolina State University.

ABBREVIATIONS

DBCO	dibenzocyclooctyne
Az	azide
NHS	hydroxysuccinimide
sNHS	sulfo-*N*-hydroxysuccinimide

TCO	*trans*-cyclooctene
ECM	extracellular matrix
GFAP	glial fibrillary acidic protein
AF488	alexa Fluor 488
ROI	region of interest
Cy7	cyanine 7
DCM	dichloromethane
DBE	dibenzyl ether
PBS	phosphate buffer saline
DMSO	dimethylsulfoxide
iv	intravascular

REFERENCES

(1). Brudno Y; Pezone MJ; Snyder TK; Uzun O; Moody CT; Aizenberg M; Mooney DJ Replenishable Drug Depot to Combat Post-Resection Cancer Recurrence. Biomaterials 2018, 178, 373–382. [PubMed: 29779862]

(2). Mejia Oneto JM; Khan I; Seebald L; Royzen M In Vivo Bioorthogonal Chemistry Enables Local Hydrogel and Systemic Pro-Drug To Treat Soft Tissue Sarcoma. ACS Cent. Sci. 2016, 2, 476–482. [PubMed: 27504494]

(3). Ries F; Klastersky J Nephrotoxicity Induced by Cancer Chemotherapy With Special Emphasis on Cisplatin Toxicity. Am. J. Kidney Dis. 1986, 8, 368–379. [PubMed: 3538860]

(4). Segota E; Bukowski RM The Promise of Targeted Therapy: Cancer Drugs Become More Specific. Cleveland Clin. J. Med 2004, 71, 551–560.

(5). Fakih M; Vincent M Adverse Events Associated with Anti-EGFR Therapies for the Treatment of Metastatic Colorectal Cancer. Curr. Oncol 2010, 17, S18–S30.

(6). Subbiah IM; Lenihan DJ; Tsimberidou AM Cardiovascular Toxicity Profiles of Vascular-Disrupting Agents. Oncologist 2011, 16, 1120–1130. [PubMed: 21742963]

(7). Smith RE; Bryant J; DeCillis A; Anderson S Acute Myeloid Leukemia and Myelodysplastic Syndrome after Doxorubicin-Cyclophosphamide Adjuvant Therapy for Operable Breast Cancer: The National Surgical Adjuvant Breast and Bowel Project Experience. J. Clin. Oncol 2003, 21, 1195–1204. [PubMed: 12663705]

(8). Kai F; Drain AP; Weaver VM The Extracellular Matrix Modulates the Metastatic Journey. Dev. Cell 2019, 49, 332–346. [PubMed: 31063753]

(9). Bhaw-Luximon A; Jhurry D New Avenues for Improving Pancreatic Ductal Adenocarcinoma (PDAC) Treatment: Selective Stroma Depletion Combined with Nano Drug Delivery. Cancer Lett. 2015, 369, 266–273. [PubMed: 26415628]

(10). Drifka CR; Loeffler AG; Mathewson K; Keikhosravi A; Eickhoff JC; Liu Y; Weber SM; John Kao W; Eliceiri KW Highly Aligned Stromal Collagen Is a Negative Prognostic Factor Following Pancreatic Ductal Adenocarcinoma Resection. Oncotarget 2016, 7, 76197. [PubMed: 27776346]

(11). Kanat O; Ertas H Shattering the Castle Walls: Anti-Stromal Therapy for Pancreatic Cancer. World J. Gastrointest. Oncol 2018, 10, 202–210. [PubMed: 30147846]

(12). Choi I-K; Strauss R; Richter M; Yun C-O; Lieber A Strategies to Increase Drug Penetration in Solid Tumors. Front. Oncol 2013, 3, 193. [PubMed: 23898462]

(13). Wolinsky JB; Colson YL; Grinstaff MW Local Drug Delivery Strategies for Cancer Treatment: Gels, Nanoparticles, Polymeric Films, Rods, and Wafers. J. Controlled Release 2012, 159, 14–26.

(14). Perry J; Chambers A; Spithoff K; Laperriere N Gliadel Wafers in the Treatment of Malignant Glioma: A Systematic Review. Curr. Oncol 2007, 14, 189. [PubMed: 17938702]

(15). Westphal M; Ram Z; Riddle V; Hilt D; Bortey E; the Executive Committee of the Gliadel Study Group. Gliadel Wafer in Initial Surgery for Malignant Glioma: Long-Term Follow-up of a Multicenter Controlled Trial. Acta Neurochir. 2006, 148, 269–275. [PubMed: 16482400]

(16). Goldberg EP; Hadba AR; Almond BA; Marotta JS Intratumoral Cancer Chemotherapy and Immunotherapy: Opportunities for Nonsystemic Preoperative Drug Delivery. J. Pharm. Pharmacol 2002, 54, 159–180. [PubMed: 11848280]

(17). Aznar MA; Tinari N; Rullán AJ; Sánchez-Paulete AR; Rodriguez-Ruiz ME; Melero I Intratumoral Delivery of Immunotherapy—Act Locally, Think Globally. J. Immunol 2017, 198, 31–39. [PubMed: 27994166]

(18). Hohenforst-Schmidt W; Zarogoulidis P; Darwiche K; Vogl T; Goldberg EP; Huang H; Simoff M; Li Q; Browning R; Turner FJ; et al. Intratumoral Chemotherapy for Lung Cancer: Re-Challenge Current Targeted Therapies. Drug Des., Dev. Ther 2013, 7, 571.

(19). Devaraj NK The Future of Bioorthogonal Chemistry. ACS Cent. Sci. 2018, 4, 952–959. [PubMed: 30159392]

(20). Brudno Y; Desai RM; Kwee BJ; Joshi NS; Aizenberg M; Mooney DJ In Vivo Targeting through Click Chemistry. ChemMedChem 2015, 10, 617–620. [PubMed: 25704998]

(21). Ji X; Pan Z; Yu B; De La Cruz LK; Zheng Y; Ke B; Wang B Click and Release: Bioorthogonal Approaches to “on-Demand” Activation of Prodrugs. Chem. Soc. Rev 2019, 48, 1077–1094. [PubMed: 30724944]

(22). Schmidt MM; Dane Wittrup K A Modeling Analysis of the Effects of Molecular Size and Binding Affinity on Tumor Targeting. Mol. Cancer Ther. 2009, 8, 2861–2871. [PubMed: 19825804]

(23). Rianna C; Radmacher M Comparison of Viscoelastic Properties of Cancer and Normal Thyroid Cells on Different Stiffness Substrates. Eur. Biophys. J 2017, 46, 309–324. [PubMed: 27645213]

(24). Goodman TT; Chen J; Matveev K; Pun SH Spatio-Temporal Modeling of Nanoparticle Delivery to Multicellular Tumor Spheroids. Biotechnol. Bioeng 2008, 101, 388. [PubMed: 18500767]

(25). Audigier C; Mansi T; Delingette H; Rapaka S; Mihalef V; Carnegie D; Boctor E; Choti M; Kamen A; Comaniciu D et al. In Parameter Estimation for Personalization of Liver Tumor Radiofrequency Ablation, Lecture Notes in Computer Science; Springer: Cham, 2014; pp 3–12.

(26). iDISCO protocol. https://idisco.info/idisco-protocol/ (accessed Feb 2, 2019).

(27). Dordi B; Pickering JP; Schönherr, H.; Julius Vancso, G. Inverted Chemical Force Microscopy: Following Interfacial Reactions on the Nanometer Scale. Eur. Polym. J 2004, 40, 939–947.

(28). Koniev O; Wagner A Correction: Developments and Recent Advancements in the Field of Endogenous Amino Acid Selective Bond Forming Reactions for Bioconjugation. Chem. Soc. Rev 2015, 44, 5743. [PubMed: 26084898]

(29). Cline GW; Hanna SB The Aminolysis of *N*-Hydroxysuccinimide Esters. A Structure-Reactivity Study. J. Am. Chem. Soc 1987, 18, 3087–3091.

(30). Imamura T; Iguchi H; Manabe T; Ohshio G; Yoshimura T; Wang Z-H; Suwa H; Ishigami S; Imamura M Quantitative Analysis of Collagen and Collagen Subtypes I, III, and V in Human Pancreatic Cancer, Tumor-Associated Chronic Pancreatitis, and Alcoholic Chronic Pancreatitis. Pancreas 1995, 11, 357–364. [PubMed: 8532652]

(31). Renier N; Wu Z; Simon DJ; Yang J; Ariel P; Tessier-Lavigne M iDISCO: A Simple, Rapid Method to Immunolabel Large Tissue Samples for Volume Imaging. Cell 2014, 159, 896–910. [PubMed: 25417164]

(32). Rossin R; Versteegen RM; Wu J; Khasanov A; Wessels HJ; Steenbergen EJ; Ten Hoeve W; Janssen HM; van Onzen AHAM; Hudson PJ; et al. Chemically Triggered Drug Release from an Antibody-Drug Conjugate Leads to Potent Antitumour Activity in Mice. Nat. Commun 2018, 9, No. 1484.

(33). Rossin R; van den Bosch SM; Ten Hoeve W; Carvelli M; Versteegen RM; Lub J; Robillard MS Highly Reactive Trans-Cyclooctene Tags with Improved Stability for Diels-Alder Chemistry in Living Systems. Bioconjugate Chem. 2013, 24, 1210–1217.

(34). Lu G; Li F; Zhang F; Huang L-L; Zhang L; Lv Y; Wei W; Xie H-Y Amplifying Nanoparticle Targeting Performance to Tumor via Diels-Alder Cycloaddition. Adv. Funct. Mater 2018, 28, No. 1707596.

(35). Miyamoto H; Murakami T; Tsuchida K; Sugino H; Miyake H; Tashiro S Tumor-Stroma Interaction of Human Pancreatic Cancer: Acquired Resistance to Anticancer Drugs and Proliferation Regulation Is Dependent on Extracellular Matrix Proteins. Pancreas 2004, 28, 38–44. [PubMed: 14707728]

(36). Moeendarbary E; Weber IP; Sheridan GK; Koser DE; Soleman S; Haenzi B; Bradbury EJ; Fawcett J; Franze K The Soft Mechanical Signature of Glial Scars in the Central Nervous System. Nat. Commun 2017, 8, No. 14787.

(37). Wang Y; Wang H; Li C-Y; Yuan F Effects of Rate, Volume, and Dose of Intratumoral Infusion on Virus Dissemination in Local Gene Delivery. Mol. Cancer Ther. 2006, 5, 362–366. [PubMed: 16505110]

(38). Jessen NA; Munk ASF; Lundgaard I; Nedergaard M The Glymphatic System: A Beginner's Guide. Neurochem. Res 2015, 40, 2583–2599. [PubMed: 25947369]

(39). Garnier L; Gkountidi A-O; Hugues S Tumor-Associated Lymphatic Vessel Features and Immunomodulatory Functions. Front. Immunol 2019, 10, 720. [PubMed: 31024552]

(40). Gee KR; Archer EA; Kang HC 4-Sulfotetrafluorophenyl (STP) Esters: New Water-Soluble Amine-Reactive Reagents for Labeling Biomolecules. Tetrahedron Lett. 1999, 40, 1471–1474.

(41). Aldwin L; Nitecki DE A Water-Soluble, Monitorable Peptide and Protein Crosslinking Agent. Anal. Biochem 1987, 164, 494–501. [PubMed: 3674396]

(42). Helio TR The Blood Brain Barrier; Nova Science Pub Incorporated, 2008.

(43). Brudno Y; Silva EA; Kearney CJ; Lewin SA; Miller A; Martinick KD; Aizenberg M; Mooney DJ Refilling Drug Delivery Depots through the Blood. Proc. Natl. Acad. Sci. U.S.A 2014, 111, 12722–12727. [PubMed: 25139997]

(44). Oneto MJM; Gupta M; Leach KJ; Lee M; Sutcliffe JL Implantable Biomaterial Based on Click Chemistry for Targeting Small Molecules. Acta Biomater. 2014, 10, 5099–5105. [PubMed: 25162537]

(45). Czuban M; Srinivasan S; Yee NA; Agustin E; Koliszak A; Miller E; Khan I; Quinones I; Noory H; Motola C; et al. Bio-Orthogonal Chemistry and Reloadable Biomaterial Enable Local Activation of Antibiotic Prodrugs and Enhance Treatments against Staphylococcus Aureus Infections. ACS Cent. Sci 2018, 4, 1624–1632. [PubMed: 30648146]

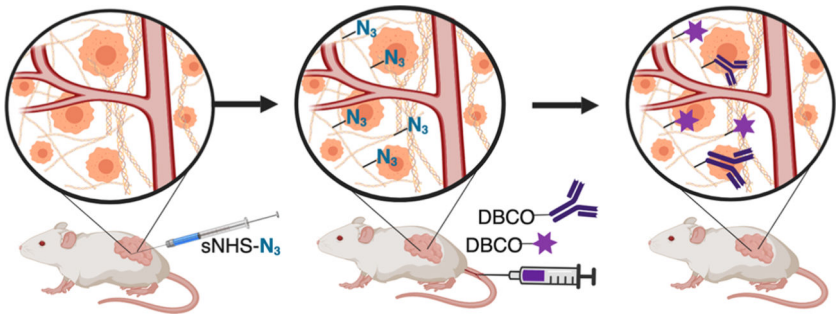

Figure 1.

ECM anchoring to introduce click motifs in target tissues. Left to middle: injections of activated NHS esters anchor azide molecules to tissue ECM. Middle to right: intravascular administration of cyclooctyne conjugated to small molecules or antibodies allows selective capture and display at tumor sites.

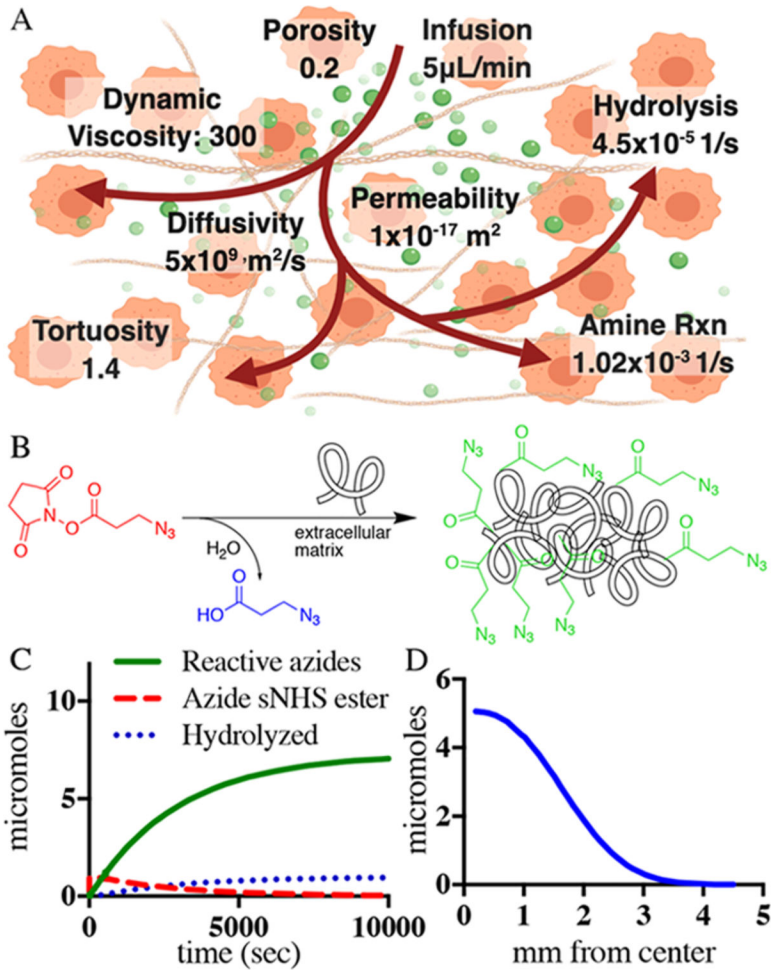

Figure 2.

Modeling of azide anchoring to tumor ECM with intratumoral fluid flow. (A) Schematic diagram of NHS-ester injection, aminolysis, and hydrolysis as well as COMSOL Multiphysics model parameters. (B) 0D model estimating the change in the concentration of the injected azide-sNHS ester, hydrolyzed species, and ECM-anchored azides over time. The expected reaction kinetics is further layered on a three-dimensional (3D) space-dependent model that leads to the results in (C). (C) Number of anchored azides available to bind to systemic DBCO molecules over mm from the center of the infusion needle in the tumor.

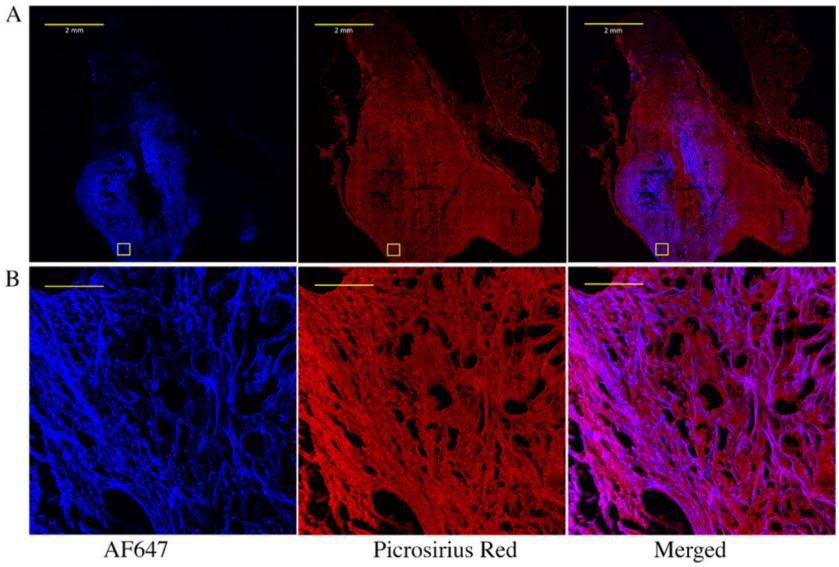

Figure 3.

Imaging NHS-ester and extracellular matrix co-localization within a pancreatic tumor. (A) Whole tumor and (B) zoom-in images of the boxed area of fluorophore-NHS-injected tumors stained for extracellular proteins with picrosirius red. Pancreatic KPC 4662 tumors were injected intratumorally with AF647 NHS ester. After 24 h, tumors were excised, fixed, sectioned, and stained with picrosirius red. The scale bars for (A) and (B) are 2 mm and 100 μm, respectively.

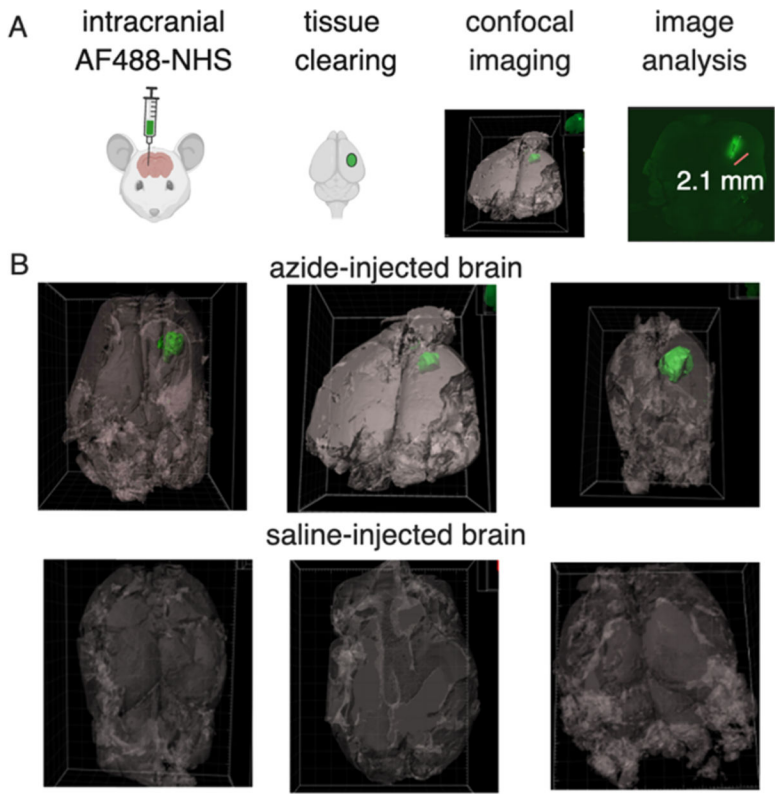

Figure 4.

Imaging NHS-ester distribution within a murine brain using model fluorescent NHS ester and tissue clearing. (A) Schematic of the azide depot visualization method from NHS injection, clearing, imaging, and analysis. (B) Representative green isosurfaces of the three Alexa Fluor 488 injected tumors and PBS-injected controls. Autofluorescence in tissues was visualized and set as a gray background.

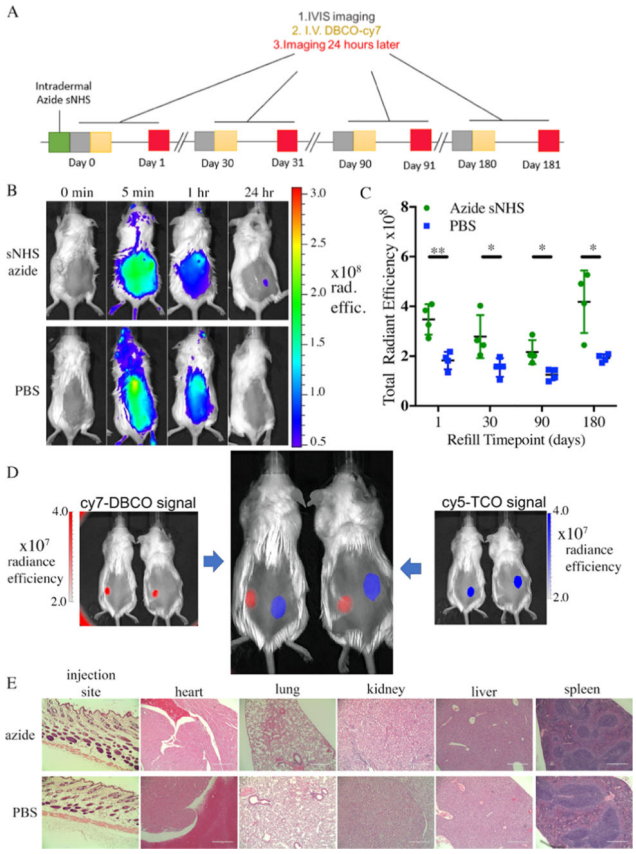

Figure 5.

Azide-sNHS ester depots allow long-term and repeated targeting with no apparent immunogenicity and are mutually compatible with tetrazine-TCO targeting for spatial separation of different regiments. (A) Timeline of systemic targeting of intradermal depots over long term. (B) Mice received an intradermal injection of azide-sNHS (50 μL of 0.2 M) or PBS and were administered iv DBCO-Cy7 and IVIS imaged before the dose and after 5 min, 1 h and 24 h. (C) Quantitation of systemic targeting of intradermal depots 1, 30, 90, and 180 days after intradermal injection of azide-sNHS (0.2 M, 50 μL) or PBS control. (D) 50 μL of methyltetrazine sNHS (right, 0.05 M) or azide-sNHS (left, 0.05 M) was injected intradermally on the dorsal flank of four mice. 1:1 DBCO-Cy7/TCO-Cy5 (200 μL) was injected iv (E) H&E staining of the skin injection site and major organs at 1 month for CD1 mice injected intradermally with 50 μL of azide-sNHS. Scale bar = 400 μm. Samples show mean ± standard error of the mean (SEM). *$p < 0.05$ by Student's t-test. See Supporting Figures 7–10 for full IVIS images.

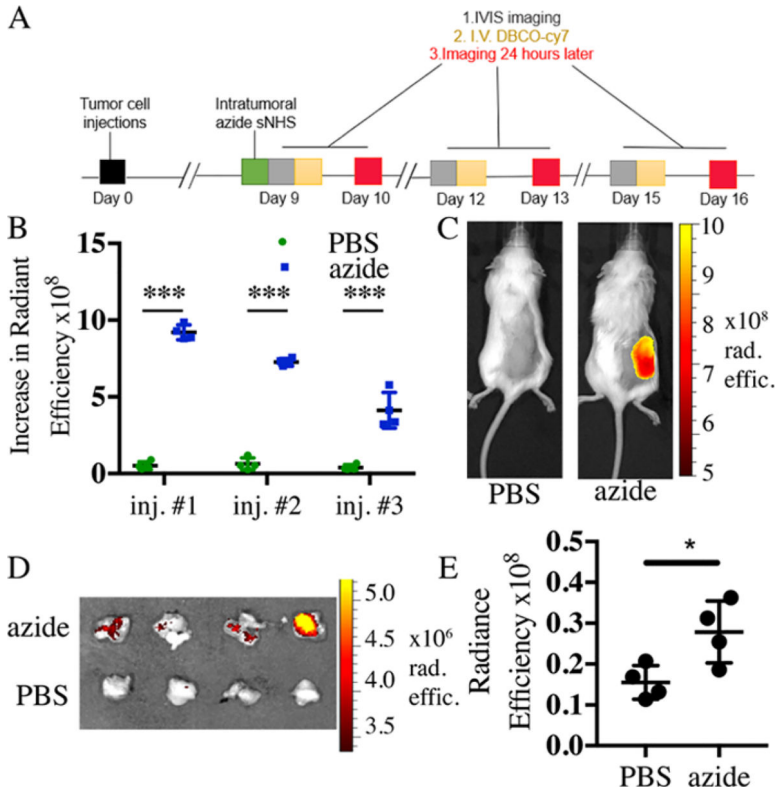

Figure 6.

Click-specific capture of small molecules and antibodies at pancreatic tumor sites. (A) Timeline for the tumor-targeting experiment for (A)–(C). Increase in radiant efficiency over tumor ROI's 24 h after iv DBCO-Cy7 administration. (C) Representative images of intratumoral azide-sNHS ester mice 24 h after iv dose of DBCO-Cy7 fluorophore. (D) Extracted azide-sNHS-infused tumors (top row) and PBS (bottom row) 24 h after iv dosing with DBCO- and Cy7-conjugated anti-PD1 antibody. (E) Quantification of radiant efficiency over tumor and underlying carcass ROI's 24 h after iv DBCO-Cy7-antibody administration. Samples show mean ± SEM. *$p < 0.05$, **$p < 0.01$, ***$p < 0.001$ by Student's *t*-test. See Supporting Figures 12–14 for full images.

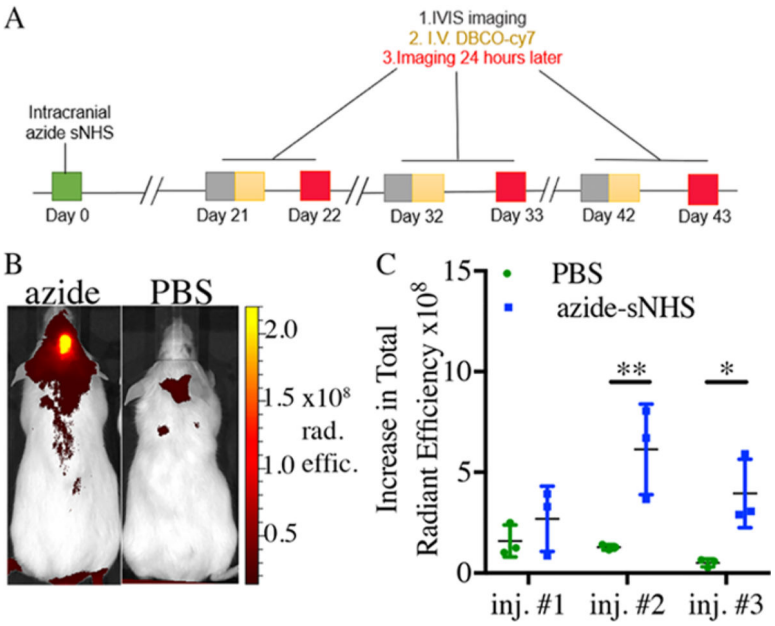

Figure 7.

Click-specific capture of small molecules in the brain. (A) Timeline of the intracranial-targeting experiment. (B) Representative images of azide-sNHS and control mice after three iv administrations of DBCO-Cy7. (C) Quantitation of intracranial ROI radiant efficiency measured 24 h after iv DBCO-Cy7 administration. Samples show mean ± SEM. *$p < 0.05$, **$p < 0.01$ by Student's *t*-test. See Supporting Figures 19–21 for full images.

Author Manuscript

Author Manuscript

Author Manuscript

Table 1.

Estimated Reacted Azide Volume and Radial Diffusion after a 50 μL Intratumoral Injection of Alexa Fluor 488 NHS Ester or PBS

	AF488 NHS mean ± SD	PBS mean ± SD
estimate reacted azide volume (μL)	12.8 ± 3.49	0
estimated radial diffusion (mm)	4.95 ± 0.816	0